Physica E 56 (2014) 183–188

Contents lists available at ScienceDirect

Physica E

journal homepage: www.elsevier.com/locate/physe

Hydrothermal synthesis and gas sensing properties of $WO_3 \cdot H_2O$ with different morphologies

Wen Zeng [a,b,c,*], Yanqiong Li [a], Bin Miao [a], Kangguan Pan [a]

[a] College of Materials Science and Engineering, Chongqing University, Chongqing 400030, China
[b] National Engineering Research Center for Magnesium Alloys, Chongqing 400030, China
[c] State Key Laboratory of Power Transmission Equipment and System Security and New Technology, Chongqing University, Chongqing 400030, China

HIGHLIGHTS

- Variety low-dimensional nano architectures were reported in the field of WO_3 via hydrothermal process.
- A growth mechanism is proposed based on comparative studies.
- Nanosheets-like WO_3 hierarchical architectures showed the excellent properties

GRAPHICAL ABSTRACT

In this work, we prepare various kinds of WO_3 low-dimensional architectures via a simple hydrothermal process, and report their growth formation mechanism and gas sensing properties.

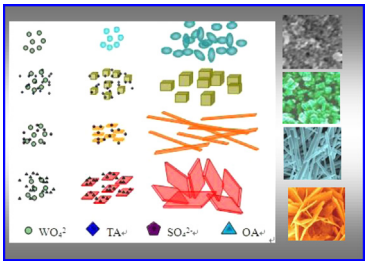

ARTICLE INFO

Article history:
Received 22 August 2013
Received in revised form
4 September 2013
Accepted 5 September 2013
Available online 18 September 2013

Keywords:
Oxides
Hydrothermal
Chemical synthesis
Morphologies
Nanostructures

ABSTRACT

$WO_3 \cdot H_2O$ with different morphologies were synthesized through hydrothermal method by adding different surfactants. The effect of surfactants on tailing morphology was investigated through XRD and SEM analyses in detail and the possible formation mechanism was discussed. Furthermore, the gas-sensing performances of obtained samples to ethanol were investigated. The results revealed that the $WO_3 \cdot H_2O$ with the hierarchical architectures assembled by nanosheets shows the highest response to ethanol among four kinds of the nanostructures WO_3. These results on the preparation, mechanism and gas sensing properties of $WO_3 \cdot H_2O$ nanostructures hold great potential for the syntheses of oxide materials with novel nanostructures and their applications.

1. Introduction

Metal oxide semiconductors with diverse morphological structure have a wide range of potential applications [1]. In particular, nano-structured metal oxide semiconductors draw a great deal of attentions due to their applications in the field of sensors, photocatalysis, electrochromic, field-emission, and solar energy devices [2–4]. In recent years, many metal oxides such as SnO_2 [5], ZnO [6], TiO_2 [7], NiO [8], MoO_3 [9], WO_3 [10] are widely investigated due to their excellent properties and potential applications. Among the numerous metal oxides investigated, tungsten oxides and its hydrates ($WO_3 \cdot \chi H_2O$) are of intense interests and have been investigated extensively for their distinctive properties.

Nanostructural materials with different morphologies have great interests due to their importance in basic scientific research and potential technology applications. Therefore, it is of critically important to synthesis $WO_3 \cdot \chi H_2O$ with well-controlled dimensionality,

* Corresponding author at: College of Materials Science and Engineering, Chongqing University, Chongqing 400030, China. Tel./fax: +86 23 65102465.
E-mail addresses: zeng_wen1982@yahoo.com.cn, wenzeng@cqu.edu.cn (W. Zeng).

1386-9477/$ - see front matter © 2013 Elsevier B.V. All rights reserved.
http://dx.doi.org/10.1016/j.physe.2013.09.005

size, morphology, and crystal structure for industrial and high-technology applications [11–13]. Many methods have been employed to control the dimensionality, size, morphology, and crystal structure of tungsten oxides, such as sol–gel, chemical vapor deposition, hard template, hydrothermal technique and so on [14–16]. Among the abundant methods, synthesis under hydrothermal conditions can provide a direct, cost-effective, one-step route to prepare nanosized tungsten oxides.

Over the past few years, much effort has been devoted to the synthesis of $WO_3 \cdot \chi H_2O$ with the morphologies of nanoparticles [17], nanocubes [18], nanorods [19], nanowires [20], nanofilms [21], nanoplates [22], nanospheres [23], and hollowsphere [24] via hydrothermal technique. All the hydrothermal synthesis routes are with the assistance of different kinds of additives which can be divided into organic surfactants and inorganic surfactants. However, the different effects of surfactants on the formation of various morphologies and their mechanism have not been investigated exactly.

Herein, varied nanostructured $WO_3 \cdot H_2O$ were prepared via a facial hydrothermal method with several kinds of surfactants such as L(+)-tartaric acid, oxalic acid, and K_2SO_4. The results show that the additive plays a significant role in the growth of $WO_3 \cdot \chi H_2O$. Then the formation mechanism of $WO_3 \cdot \chi H_2O$ with the morphologies of nanocubes, nanobelts and nanosheets were assumed and graphic presented. It is hoped that this study would help to further understand the growth mechanism of tungsten oxides and its hydrates. Moreover, we also investigate the gas sensing properties of different morphologies to ethanol.

2. Experimental

2.1. Synthesis of samples

All chemicals are purchased from Chongqing Chuandong Chemical Reagent Co. Ltd and used without further purification.

In a typical route, 0.66 g of sodium tungstate ($Na_2WO_4 \cdot 2H_2O$) and 0.4 g of citric acid were mixed and dissolved into 40 ml of distilled water under 10 min of magnetic stirring to form transparent solution. Then several milliliters of 3 M HCl aqueous solution was introduced into the aqueous solution, resulting in yellow precipitation was obtained (adjust the pH value to 1). After 20 min of stirring, the solution was transferred into a 50 ml Teflon-lined stainless steel autoclave, which was sealed and treated at 160 °C for 12 h, and then cooled to room temperature naturally. The obtained precipitates were separated by centrifugation, wash several times with distilled water and absolute ethanol and then dried in vacuum at 60 °C for 4 h.

The as-prepared yellow precipitates using no additive was named samples A, while powders obtained with the addition of L(+)-tartaric acid (TA), potassium sulfate (K_2SO_4) and oxalic acid (OA) were named as samples B, C and D, separately.

2.2. Characterization of samples

The phase and crystallinity of the as-obtained samples were characterized by X-ray diffraction (Rigaku, D/Max- 1200X dffractometer) using CuKα radiation operated at 30 kV and 100 mA and with a step size of 0.05° and a scanning speed of 0.2 °/min. The morphologies and sizes of these nanosized powders were investigated by a field emission scanning electron microscope, FESEM (Nova 400 Nano operate at 10.0 kV).

2.3. Fabrication of gas sensor

The prepared powders were dispersed in distilled water to form pastes with the assistance of untrasonication. The pastes were then coated onto an alumina ceramic tube, on which a pair of gold electrodes was loaded in advance at each end point (Fig. 1a). Further heat treatment at 350 °C for 3 h was essential to remove the organic binder and enhance the mechanical adhesion between the pastes and the tube. Finally, a Ni–Cr wire was inserted into the tube as a heater. Gas sensors were fabricated by welding the heater and the tube on the sensor pedestal. The target gas was introduced by injecting certain amount of that gas into the glass chamber. The operating temperature could be adjusted via varying the heating voltage (V_h). A load resistor (R_L) was connected to the electric circuit of the gas sensor (Fig. 1b).

2.4. Gas sensing measurement

Gas-sensing properties were measured using HW-30A gas sensitivity instrument (Hanwei Electronics Co. Ltd PR China). The resistance (R_S) of the gas sensor was estimated from $R_S = R_L(V_c - V_{out})/V_{out}$, where V_c and V_{out} were the circuit and output voltage, respectively (Fig. 1b). In this paper, we described the sensitivity as gas response (S), which was defined as $S = R_g/R_a$, where R_a and R_g were resistances of the sensors in air and ethanol vapor, respectively [25,26].

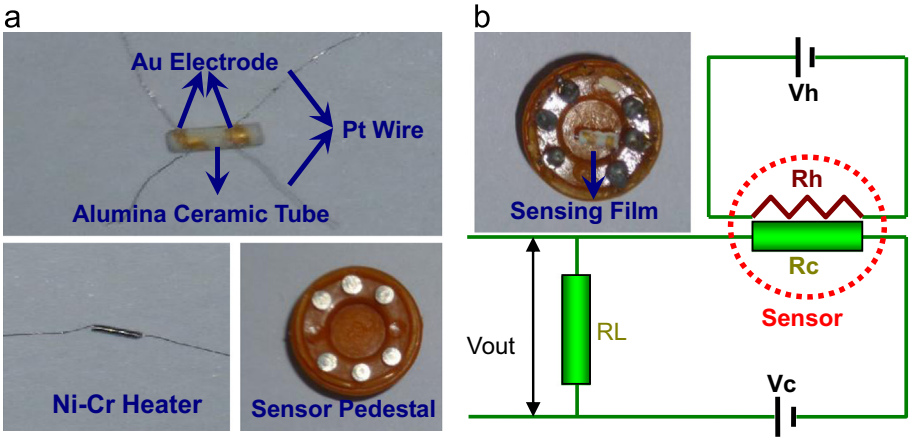

Fig. 1. (a) Scheme of the gas sensor configuration and (b) diagram of sensor and measurement electric circuit.